NTNU – Trondheim
Norwegian University of
Science and Technology

Velocity error induced by unevenly sampling wind radars

Kjetil Landgraff Ekern

Master of Science in Physics and Mathematics
Submission date: Januar 2014
Supervisor: Patrick Joseph Espy, IFY

Norwegian University of Science and Technology
Department of Physics

Summary

Measurements of atmospheric winds in the mesosphere and lower thermosphere (MLT) region using a SKiYMET radar started in Trondheim (63.4° N, 10.4° E) in September 2012. This meteor radar utilizes the ionized trail from meteors entering the atmosphere to observe a line of sight velocity og the wind, distance from radar as well as zenith and asimuth angle of the wind. By collecting data over a period of time (typically bins of one hour) one can use these data to deduct the zonal and meridional component of the atmospheric wind during that period.
The number of meteors that are observed during this period of time will have daily and seasonal variations and at times the centroid time of arrival of the meteors can differ from the centroid time of the bin (bin time). Since the bin time is commonly used for analysis of the wind measurements, this thesis analyses the error induced by assuming the bin time is the correct time. By looking at 11 months of data the typical difference between real time and bin time has been analyzed, and an induced wind error has been deducted by comparing the measured wind to a linearly interpolated wind using the real time of arrival. Using 3 hour bins the mean magnitude of the time error was found to be 9-11.7 minutes at the altitudes 81-99 km (6 km altitude bins). This leads to a mean induced error of 2.5 m/s at 81-87 km, 5.6 m/s at 87-93 km and 5.7 m/s at 91-99 km. In 5.4% of the measured components this time induced wind error was found to be larger then the error in the measured wind components.
The connection between the time error and the meteor count rate was analyzed, and also the connection between the meteor count rate and the atmospheric ionisation measure Kp. Two example analyses were done using both real time and bin time for the measurements. The semidiurnal atmospheric tide was found for 11.09.2012-11.08.2013 each day using 3-hour bins, and also for October 2013 using 1-hour bins. The difference between the two approaches was generally low in both examples, however significant differences was observed.
Although the errors due to the two time bases are small for the 35 kW system at Dragvoll, where high meteor count rates (typically between 8000-17000 meteors per day) ensure a more even distribution across the bin, the differences between these are likely to be more prevalent for a typical low power system (6kW), where the meteor count rates can be up to a factor of four lower. Thus, for comparisons between system based on different count rates, winds and tides based on real time should be used.

Sammendrag

Målinger av atmosfæriske vinder i mesosfære- og den lavere termosfære-regionen (MLT-regionen) ved bruk av SKiYMET radar, ble påbegynt i Trondheim (63.4° N, 10.4° E) i september 2012. Denne typen radar benytter seg av ioniserte spor etterlatt av meteorer som entrer atmosfæren og observerer v.h.a. dette hastigheten på vinden i synsretningen, avstanden fra radaren, zenit og asimut vinkel for hver meteor. Man kan dele disse dataene opp i tidsperioder (typisk på en time og bruke dem til å finne en zonal (nord-sør) og en meridional (øst - vest) vindkomponent for denne tidsperioden.
Antallet meteorer som blir observert i løpet av denne perioden vil variere med både sesong og tid på dagen, noe som fører til at sentraltiden for meteorenes ankomst (realtid) kan variere fra sentraltiden til tidsperioden (midttid). Siden denne midttiden ofte blir brukt til analyser og vindmålinger, har denne oppgaven satt fokus på hva slags feil det medfører å gjøre antakelsen om at midttid er riktig. Ved å studere elleve måneder data har den typiske forskjellen mellom realtid og midttid blitt analysert, og en tidsindusert vindfeil har blitt funnet ved å sammenlikne den målte vinden i midttiden med en lineær interpolasjon gjort med den målte vinden og realtiden.
Ved å dele dataene inn i perioder på tre timer ble den gjennomsnittlige størrelsen på tidsfeilen funnet til å være fra 9-11.7 minutter i 81-99 km høyde (høydemessig oppdeling på 6 km). Dette fører til at den tidsinduserte vindfeilen får en gjennomsnittlig størrelse på 2.5 m/s for 81-87 km, 5.6 m/s for 87-93 km og 5.7 m/s for 91-99 km. høyde. I 5.4% av vindkomponentmålingene ble denne tidsinduserte vindfeilen funnet å være større enn feilen fra selve målingene av vindkomponentene.
Sammenhengen mellom tidsfeil og antallet observerte meteorer ble også analysert, såvel som sammenhengen mellom antallet meteorer og den atmosfæriske måleverdien Kp.
Det ble gjort to eksempelanalyser, hvor både realtid og midttid ligger til grunn for målingene. En semidiurnal atmosfærisk tidevannsbølge har blitt funnet for hver dag i perioden 11.09.2012-11.08-2013, med tidsinndeling på tre timer, og også for oktober 2013, da med tidsinndeling på en time. Forskjellen mellom resultatene fra hver metode var generelt lav i begge analysene, men det ble også observert måleresultater med signifikante forskjeller.
Selv om feilen på grunn av de to tidsbasisene er liten ved bruk av 35 kilowattssystemet på Dragvoll, hvor det høye daglige meteorantallet (vanligvis mellom 8000 og 17 000 meteorer/dag) sørger for en jevn distribusjon av meteorer i tidsperiodene, er det sannsynlig at denne forskjellen er større for et typisk laveffektanlegg (6kilowatt), hvor det daglige meteorantallet kan være så mye som en faktor fire lavere. Derfor bør vinder og atmosfæriske tidevannsbølger baseres på realtid, dersom disse skal sammenliknes med resultater fra systemer basert på forskjellig daglige meteorantall.

Acknowledgments

This report is the product of TFY4900, Master Thesis in Physics at the Norwegian University of Science and Technology. I would like to thank Prof. Patrick J. Espy for all the knowledge he has shared with me throughout the work with this thesis.
I would also like to thank my fellow students for always brightening my day, with a special mention of Magnus Svennevik, my personal trainer and Matlab error detection partner. Not to mention Endre G. Ofstad, who provided me with a beautiful picture of the aurora borealis.

Table of Contents

Summary i

Summary ii

Preface iii

Table of Contents v

List of Tables vii

List of Figures xi

1 Introduction 1

2 Theory 3

3 Method 9

4 Results and analysis 13

5 Conclusion and further work 39

Bibliography 40

List of Tables

4.1 Average number of meteors at the different altitudes in the period 11. September 2012 - 11. August 2013. The error given is the standard deviation in the data. 16
4.2 Average magnitude of time error at different altitudes 11. September 2012 - 11.August 2013. Error is the standard deviation. 19
4.3 List of averages of the wind error induced by differences between real time and middle time. The error in these numbers are the standard deviation in the data. 23
4.4 Average magnitude of the wind error as result of real time deviation from middle time. Errors are standard deviations from the data. 23
4.5 This table contains the mean standard deviation from the fitting of the wind data points. 23

List of Figures

2.1 This is a screenshot of the atmospheric group's website at a typical day, showing the meteor-flux-veriation through the day, the height distribution and the angular distribution of detected meteors. Homepage: $http://home.phys.ntnu.no/brukdef/prosjekter/atmosfys/web-pages/SKiYMET-wind.php$ 4

2.2 Schematic overview of the SKiYMET meteor radar setup. The receiving antennas are to the right and the transmitting antennas to the left. Source: Genesis software 4

2.3 Example of output file from the SKYiMET meteor radar. 5

2.4 Example picture of how the data are presented at the Atmospheric group at NTNU's web page 5

2.5 Electron precipitation energies and ionisation rates. Source [Jur85] 7

3.1 (a) Illustration plot with generated values. The real time (blue dots) values are generated by edding a gaussian random value to the bin time. A sine wave is then created on the real time, and the same values are plotted at bin times. (b) Magnitude of the error induced by plotting the generated real time values on the bin times. 9

4.1 Kp and Ap values for the period 11.09.2012 - 20.08-2013. (a) Kp values. +/- values of Kp is found over/under the value, so Kp=6- is represented as Kp=5.7. (b) Equivalent Ap values to the Kp values in (a). Source for the data:[SWP] 15

4.2 Scatter of Kp vs. N_{rel} at 81-86 km, 86-93 km and 93-99 km. 16

4.3 Average N_{rel} as function of Kp plotted with SME. (a) 93-99 km, (b) 87-93 km, (c) 81-87 km 17

4.4 Kp and mean N_{rel} for Kp=3+ - 7-. (a) 93-99 km, (b) 87-93 km, (c) 81-87 km 18

4.5 Example plot of the induced wind error from January 19th 2013, 93-99 km. (a) Blue: measured wind plotted and interpolated with real time. Red: Measured wind plotted at bin time with error from the measurement. (b) Difference between the measured wind and the linearly interpolated wind at bin time. 21
4.6 This plot shows the magnitude of the difference between real time and fixed time in the 93-96 km range. The red lines in the plot depict one and two standard deviations of this data. (a) 81-87 km, (b) 87-93 km, (c) 93-99 km. 22
4.7 The time errors have been sorted after number of meteors, as 0-50, 50-100, ... 450-500 and >500. Both the average magnitude of the time error and the average of N have been found for each segment, so the time errors are plotted at their respective mean N. The errorbars show the standard mean error of the real time used for each average. Altitudes: (a) 93-99 km, (b) 87-93 km, (c) 81-87 km. 24
4.8 The time errors have been sorted after number of meteors, as 0-50, 50-100, ... 450-500 and >500. The real time and the number of meteors were averaged and plotted at their real number in the graphs. The errorbars show the standard deviation of the real times used in each average. Altitudes: (a) 93-99 km, (b) 87-93 km, (c) 81-87 km. 25
4.9 Difference between the amplitudes found in figure 4.10. The difference is the amplitude found using real time minus the amplitude found using middle time. (a) Zonal semidiurnal differences. (b) Meridional semidiurnal differences. 27
4.10 Amplitudes found for the zonal semidiurnal tide Sept. 11th 2012 - Aug 11th 2013. (a) Amplitudes found using middle times. (b) Amplitudes found using real times. 28
4.11 Amplitudes found for the meridional semidiurnal tide Sept. 11th 2012 - Aug 11th 2013. (a) Amplitudes found using middle times. (b) Amplitudes found using real times. 29
4.12 σ-error of the fitted amplitudes found in figure 4.10. (a) Middle time. (b) Real time. 30
4.13 σ-error of the fitted amplitudes found in figure 4.11 (a) Middle time. (b) Real time 31
4.14 Phase of the semidiurnal waves fitted from 11.092012 - 11.08.2013. (a)Zonal, real time, (b) Zonal, bin time, (c) Meridional, real time, (d) Meridional, bin time 31
4.15 Plot of the zonal component of the wind at 93-99 km around 19.01.2013. . 32
4.16 Difference between the semidiurnal amplitudes found for October 2013 using real time and middle time. (a) Zonal semidiurnal differences. (b) Meridional semidiurnal differences. 34
4.17 Amplitudes found for the semidiurnal tide October 2013 using fixed hourly time points. (a) Zonal, (b) Meridional 35
4.18 Amplitudes found for the semidiurnal side October 2013 using average time points. (a) Zonal, (b) Meridional 36

4.19 Zonal σ error of the amplitudes in figures 4.18 and 4.17. (a) Bin time, (b) Real time 37
4.20 Meridional σ error of the amplitudes in figures 4.18 and 4.17. (a) Bin time, (b) Real time 38
4.21 Phase of the semidiurnal tide October 2013 using 1-hour bins. (a) Zonal, real time, (b) Zonal, bin time, (c) Meridional, real time, (d) Meridional, bin time. 38

Chapter 1

Introduction

By observing the ionization trail from meteors entering the atmosphere one can measure the line of sight (LOS) wind velocity at meteor ablation altitudes (75-100 km). Over the course of an hour enough meteors are normally detected, so that a zonal (north-south) and meridional (east-west) wind can be deduced from the individual LOS velocities. The time for the measurement is typically set to be the centre time of this hourly averaging bin of the wind. The meteors occur randomly during the hour-long periods and at times the centroid time of the meteors (real time) may differ substantially from the centroid time of the hourly bin (middle time). The number of meteors detected may also be affected by the ionisation from electron precipitation, further skewing this effect.
In this thesis we will examine the effect of the random meteor arrival times on the hourly winds and the extracted tidal amplitudes and phases. We also examine the relationship between the variations of the meteor count rate and the geomagnetic indices to see if auroral activity can influence the discrepancies between these two time bases.

Chapter 2

Theory

The SKYiMET meteor radar

The SKiYMET radar system has been described in detail by Hocking ([Hoc01]), and the salient points discussed there are presented here.
The data upon which this project is based comes from a SKiYMET radar located at Dragvoll, Trondheim. This piece of equipment utilizes eight transmitter antennas and five receiver antennas that receive the signals reflected from the ionized trails left behind by meteors entering the atmosphere. These trails lasts for up to about four seconds as they burn up in the atmosphere, and during this time they will drift with the wind. The extracted information includes the line of sight velocity of the trail, distance from the radar, azimuth angle, zenith angle and ambiguity. Due to the high power and the number of transmitter and receiver antennas the SKiYMET radar can detect meteors in a great span of zenith angle, and it can receive data from many more meteors each day, compared to older types of radars. This gives more possibilities when it comes to treating this information. The transmitting antennas transmit at 34.21 MHz and a repetition rate of about 1 kHz, while the receiving antennas are sampled at 128 samples in 4s (wavelength $\lambda \approx 9m$). The eight transmitting antennas are placed in an octagon with about 1λ of distance to their nearest neighbor. This setup is to focus the radiation towards zenith angle 10°-90°, and ignore the area around zenith. This setup transmits most of the power into zenith angles between 18° and 50°, with a secondary maximum between 60° and 90°

The receiving antennas are set up as a cross with one antenna in the middle, and the four placed around it with 90° between them (as in figure 2.2). Two of the antennas are placed at a distance of $r = 2\lambda$ away from the middle antenna, while the two others are placed at a distance of $r = 2.5\lambda$.

Using this setup, the difference in phase at the different antennas makes it possible to determine the position of the detected meteor. This is done my predicting several positions

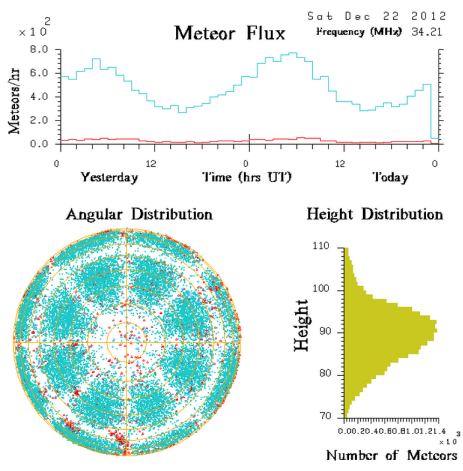

Figure 2.1: This is a screenshot of the atmospheric group's website at a typical day, showing the meteor-flux-veriation through the day, the height distribution and the angular distribution of detected meteors. Homepage: $http : //home.phys.ntnu.no/brukdef/prosjekter/atmosfys/web - pages/SKiYMET - wind.php$

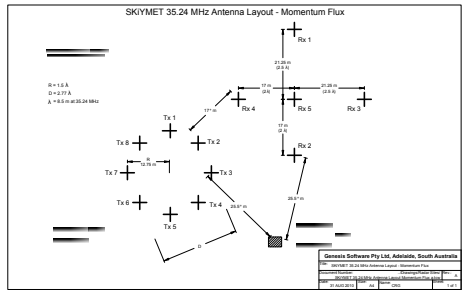

Figure 2.2: Schematic overview of the SKiYMET meteor radar setup. The receiving antennas are to the right and the transmitting antennas to the left. Source: Genesis software

where the meteor can have been detected, and choosing the one which gives the lowest error, given that the error is smaller then a given threshold. If two or more positions give the lowest error, the meteor is marked as ambiguous and the number of ambiguous points is noted in the output file.

The number of meteors detected by the radar varies from day to day and also within the day, with an average of about 15,000 detections a day. This meteor flux varies through the day, since the earth rotates around its axis as well as around the sun and it is highest when the earth's orbital and rotational tangential velocities lie along the orbital path near dawn. Conversely, the number of meteors swept is minimum near dusk. This means that the tilt of the earth relative to the earth's orbit will affect the number of meteors we can detect.

For this reason one can expect to detect more meteors in the summer half of the year, then during the winter.
When detecting meteors, the radar processes received signals and determines whether or not the detection of an event is a meteor. A possible meteor event will be compared to the average signal around that time. If the event differs from the mean by n standard deviations, where n is user defined, the signal will be processed further. The rate at which the time rises and lifetime of the event is also analyzed. If the rise is too slow or the lifetime is too long (generally 2-3s), the event is rejected. This removes airplanes, E-type echoes and other non-meteor contaminants to the signal.

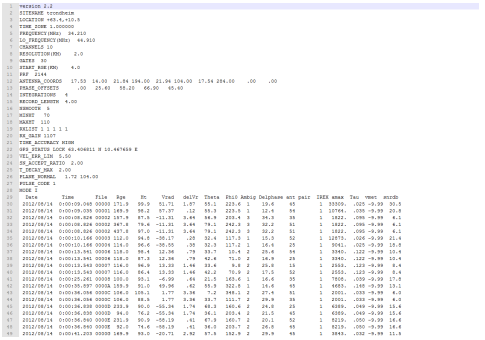

Figure 2.3: Example of output file from the SKYiMET meteor radar.

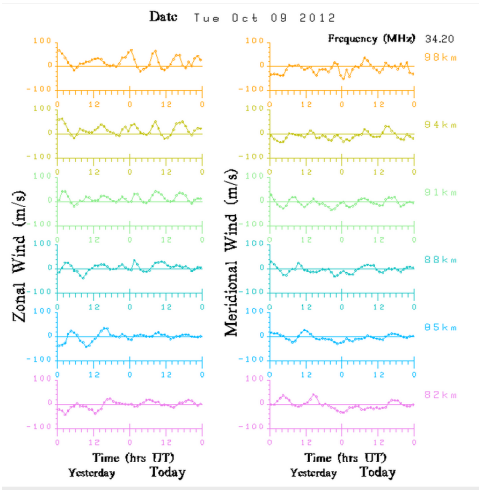

Figure 2.4: Example picture of how the data are presented at the Atmospheric group at NTNU's web page

Electron precipitation

Electron precipitation is another source to the ionisation and dissociation in the atmosphere [TVS$^+$09]. The particle flux and intensity of these electrons varies with time which in turn creates a variation in the ionisation of the atmosphere. During solar events like high speed solar wind streams and coronal mass ejections, there is an increase in the geomagnetic activity and energy inputs to the magnetosphere. Electrons trapped on the geomagnetic field lines are energized and begin to accelerate towards the earth. These electrons penetrate down to different heights according to the amount of energy they have. From figure 2.5 one can see that the electrons which penetrate the atmosphere down to 80-100 km are generally a distribution of electrons with energy above 10 keV. The ionisation during daytime in the atmosphere is around 10^5cm^{-1} at 100 km going down to around 10^4cm^{-1} at 80 km. During night these numbers go down to 10^3-10^4 [Jur85]. From figure 2.5 we see that the electron precipitation at 100 km altitude from electrons with energy 10 keV can be of the order 10^4. This means that the auroral precipitation of electrons during nighttime can effectively bring the background ionisation level up to daytime values, and increase the background ionisation during daytime by close to a factor of two.

K_p and A_p are measurements widely used as a numeric description of the magnetic activity in the atmosphere. K_p, the planetary K index, is a global value of the activity and is calculated as the 3 hour average of the 12 individual station values K_s, that are observed at geomagnetic latitudes between 43° and 63^{cirk}. The irregular variations of standard magnetograms at a given observatory are measured and then standarized to the value K_s from tables in order to remove seasonal behavior characteristic for the station.
K_p ranges from 0-9 and goes via 0_0, 0+, 1-, 1_0 ... 9_0 logarithmically.
A_p is a linearized version of K_p that ranges from 0 (K_p=0) to 400 (K_p=9_0).

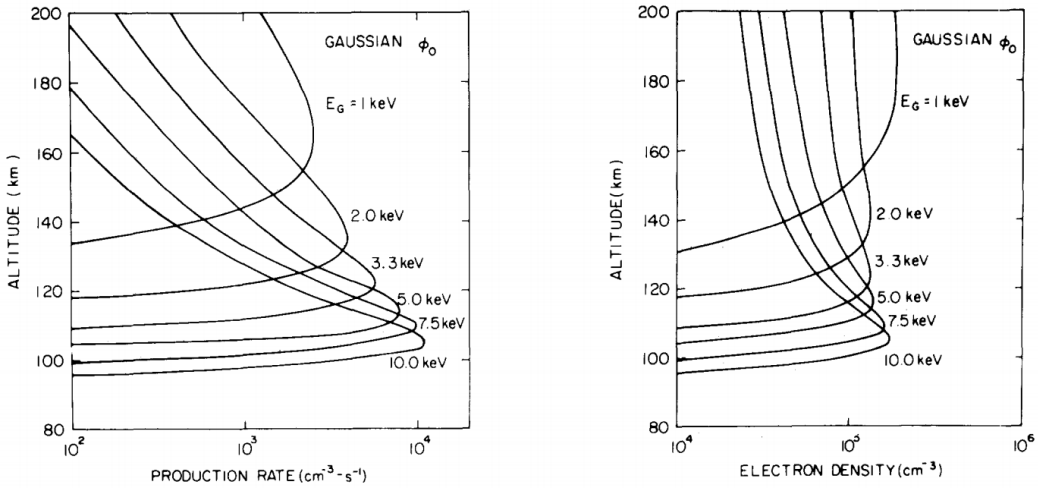

Figure 2.5: Electron precipitation energies and ionisation rates. Source [Jur85]

Atmospheric tides

Tidal oscillations are a well known thermally driven phenomenon observed in the atmosphere [Lie09], [Lin79], [For09]. During the day there is heating of the atmosphere by the absorption by H_2O and O_3, however there is no heating when the sun is down. When the atmosphere is heated, it expands which causes a pressure gradient and a forcing of the wind. This on/off nature of the atmospheric heating means this forcing cannot be explained by a single sinusoidal wave, and must instead be described by a Fourier series. The components of this Fourier series are what we can observe as the tidal oscillations in the atmospheric wind. Mathematically the heating can be described by the following equation, as it also depends on the altitude and latitude:
$J_\lambda(t) = \sum_n A_n(z,\theta,\lambda) cos(\frac{n2\pi t}{24} + \phi_n(z,\theta)$
where different values of n separate the different components. These are called diurnal ($n = 1$), semidiurnal ($n = 2$), terdiurnal ($n = 3$) tides and so on.

The latitudinal dependence of the tidal waves is the solution of Laplace's tidal equations[Lin79]. This solution consists of eigenfunctions called Hough functions and their associated eigenvalues or separation constants. By expanding the forcing in terms of these Hough functions one can find the response to the forcing by each eigenfunction, also referred to as equivalent depth. For the migrating semidiurnal tide, the Hough functions are similar to the Lagrange polynomials of order two. All the Hough functions for the semidiurnal tide have positive equivalent depths. For the migrating diurnal tide there are two dominating sets of Hough functions. One with relatively small positive depths which is restricted to each side of the equator to latitudes, $\theta = 30^\circ$. The other set has negative equivalent depth's and is situated pole-wards from $\theta = 30^\circ$. The reason for this limit is that pole-wards from $\theta = 30^\circ$ the Coriolis parameter exceeds the frequency of the diurnal tide. Because of this we can see the situation that the semidiurnal tide is more dominant then the diurnal tide at some latitudes. The semidiurnal is generally the dominant tidal wave over Dragvoll, which is where the radar used for observations in this project is situated.

Chapter 3

Method

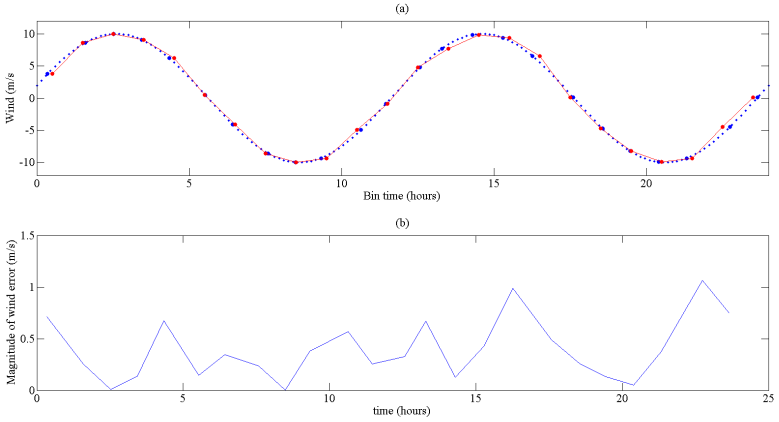

Figure 3.1: (a) Illustration plot with generated values. The real time (blue dots) values are generated by edding a gaussian random value to the bin time. A sine wave is then created on the real time, and the same values are plotted at bin times. (b) Magnitude of the error induced by plotting the generated real time values on the bin times.

Wind speed and the time

In order to find the wind speed a Matlab routine was used. By assuming no vertical component of the wind a U (zonal) and V (meridional) component of the wind was fitted to data from the SKiYMET radar by using
$V_{LOS} = U \cdot cos(\theta)cos(\phi) + V \cdot sin(\theta)sin(\phi)$
Here V_{LOS} are the line of sight velocities, θ are the zenith angles and ϕ are the azimuth angles of meteors detected in the desired height and time. The meteors were sorted by time

of arrival and altitude in three hour at a time and altitudes 81-87 km, 87-93 km and 93-99 km. The choice of three hours was done in order to work well when analyzing them with the Kp values, which are given for three hours at a time. The wind components were saved for analysis together 2σ error from the fit, average time of arrival for the meteors used in the fit (real time), standard deviation from the fit of the components for the time, average time of arrival for the meteors used in the fit (real time) and also the number of meteors for each data for the wind components. Real time refers to the mean time of arrival for the meteors so the arrival timestring from the data were converted into decimal numbers before the average was taken.
As the real time of the sample bin could differ from the middle time of the 3-hour sample bin which is often used for analysis (1 hour bins for the October semidiurnal analysis), a time induced error was also found. This was done by linearly interpolating the wind speeds at real times, before finding the difference between this at the middle time and the wind speed which was found.

Finding the average relative number of meteors N_{rel}
The average relative number of meteors was used for some analysis. This is the number of meteors in a given hour relative to the surrounding days. Since the number of detected meteors varies throughout the day[YASM09a] a simple averaging does not suffice, and the average number of meteors at that time of day in the days around is therefore used. In order to find these averages, the number of meteors for each hour of the day in question $\pm$15 days was used. The number of meteors were stored in 3 hour bins, as this is the number of hours Kp is given for, which means there was 8 bins for each day. The 1st bin in the day was found relative to the averages of the 1st bin in each of the days before and after, then the 2nd was found relative to the 2nd bin in each day before and after, and so on. When this was done for all 8 bins, the first of the 31 days would be removed, the day after the last would be added and the whole routine would repeat itself for the day in the middle. This was done over the whole time period 11.09.2012 to 11.08.2013, yielding 10 months of values for N_{rel}.

Semidiurnal tide

A semidiurnal fit was done to see what impact the difference between using the real time and the middle time might have on an analysis like that. In order to find the semidiurnal tide a fit of a twelve hour cosine wave was done with the equation
$U = Acos(\omega t + \phi)$
where A is the semidiurnal amplitude, t is the time in hours, U either the zonal or meridional component of the wind and ϕ the phase of the wave. The ω used was the standard $\frac{2\pi}{12}$ for a twelve hour wave.
By doing the routine separately for the real time and the middle time for each time interval one could examine the difference between the results from these two approaches. For each fit the amplitude, σ-error, phase, $sigma$-phase error, constant and $sigma$-constant error was stored in order to be analyzed. The 2σ-error in the fit for U and V was used as a weighting when finding the amplitude as
$W = \frac{1}{2\sigma}$.

This was done for two periods of time, 11.09.2012-11.08.2013 and 01.10.2013-30.10.2013. In the first period the wind speeds were given with 3 hour bins and three 6km bins for the altitude. In the second period hourly bins were used for the time and six 3km bins were used for the altitudes. The altitude range in both analyses was 81-99 km.

Chapter 4

Results and analysis

Kp and number of meteors The average number of meteors for each 3 hour period can be found in table 4.1. This shows that in general there are more meteors arriving in the 86-93 km range then there is in the 81-86 km range and the 93-99 km region, with the least amount of meteors in the 93-99 km region. This number is a general description over the whole period from 11.09.2012-11.08.2013, and does not take into account the variation of number of meteors during the day[SBHM10]. In order to deal with this and the high standard deviation in the number of meteors in general, a relative number of meteors in a time interval on a day (N_{rel}), was used to compare with the Kp-fluctiations. N_{rel} is the number of meteors at a time divided by the average number of meteors at that time of day over a period of 31 days around the day in question (the day in question $\pm$15 days. In order to see if there is a connection between the Kp, which can be seen in figure 4.1 value at a given hour and the number of meteors detected, the N_{rel} values were sorted and averaged according to the Kp value at the time. These can be seen in figures 4.3(a)-4 (scatter plots before the mean was taken can be seen in figure 4.2). There was only one incident where Kp=7 through in the period of time that was examined in this thesis, so the significance of this is close to zero for further analysis. This point is therefore removed from figure 4.4.
To see auroral effects at the latitude of the radar at Dragvoll, Kp should have a value of at least 3 [Jur85]. Therefore it is interesting to see if there is a connection between N_{rel} when this occurs. By only analyzing N when $3 > N_{rel} > 7$ which can be seen in figure 4.4, it becomes clear that Kp has no impact it the 81-86 km region, however in the other two regions there is a decline in the mean value for the other two regions. When taking into account the standard mean error for each value vs Kp there is a tendency in the 93-99 km region of a downwards slope as a function for N_{rel} vs Kp. An interesting note is to see that the maximum in this altitude lies around Kp=4_0 and $N_{rel} > 1$ around these Kp values. The lowest value for the average N_{rel} is found in the 86-93 km region with Kp =7- and N_{rel}=0.87$\pm$0.14.
In order to see if there really is a connection between the two, one should try using a much longer dataset. That would probably increase the number of times the Kp value is above 3 and close to 7 and in this way make all the statistics more accurate. The radar at Dragvoll

began producing meteor data in September 2012, so to go further back in time to increase the amount of data at the time of this thesis was difficult.
The data from September/October 2013 could be used to get a slightly larger set of data, however there was quite a few days of downtime on the radar in late August, so there would be a big gap in the data set. Considering there may also be yearly variations in how this effect behaves it was simply more practical and accurate to use the 11 months of more or less continuous data that was available in this thesis (some days through the period have a few hours of downtime on the radar, however nothing close to what happened in August).

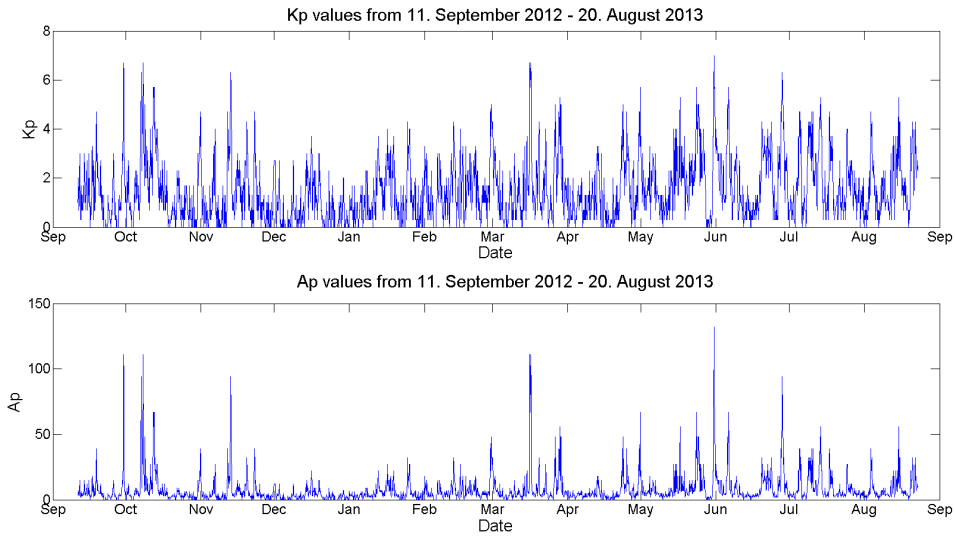

Figure 4.1: Kp and Ap values for the period 11.09.2012 - 20.08-2013. (a) Kp values. +/- values of Kp is found over/under the value, so Kp=6- is represented as Kp=5.7. (b) Equivalent Ap values to the Kp values in (a). Source for the data:[SWP]

Altitude (km)	**Average number of meteors** (#)
81-86	250±100
86-93	427±194
93-99	184±89

Table 4.1: Average number of meteors at the different altitudes in the period 11. September 2012 - 11. August 2013. The error given is the standard deviation in the data.

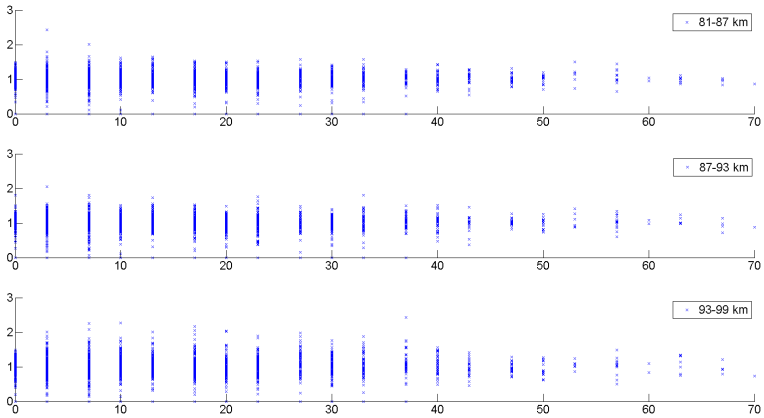

Figure 4.2: Scatter of Kp vs. N_{rel} at 81-86 km, 86-93 km and 93-99 km.

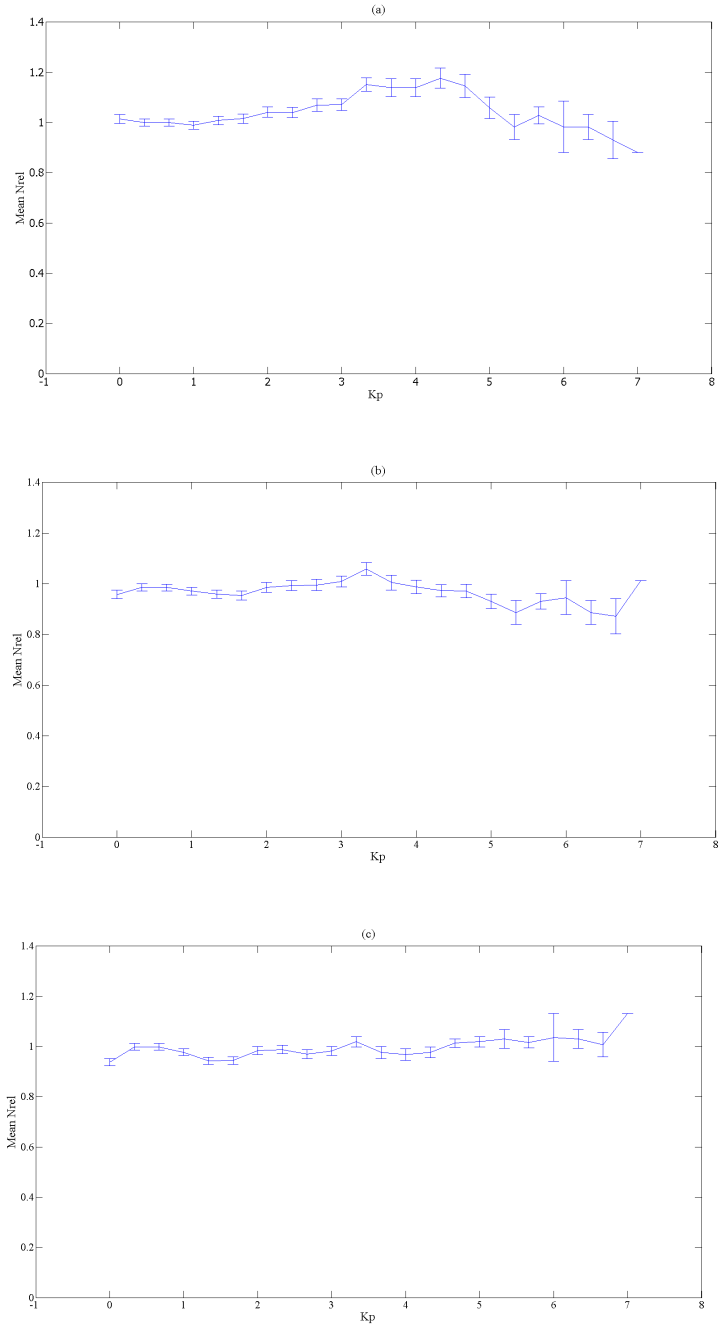

Figure 4.3: Average N_{rel} as function of Kp plotted with SME. (a) 93-99 km, (b) 87-93 km, (c) 81-87 km

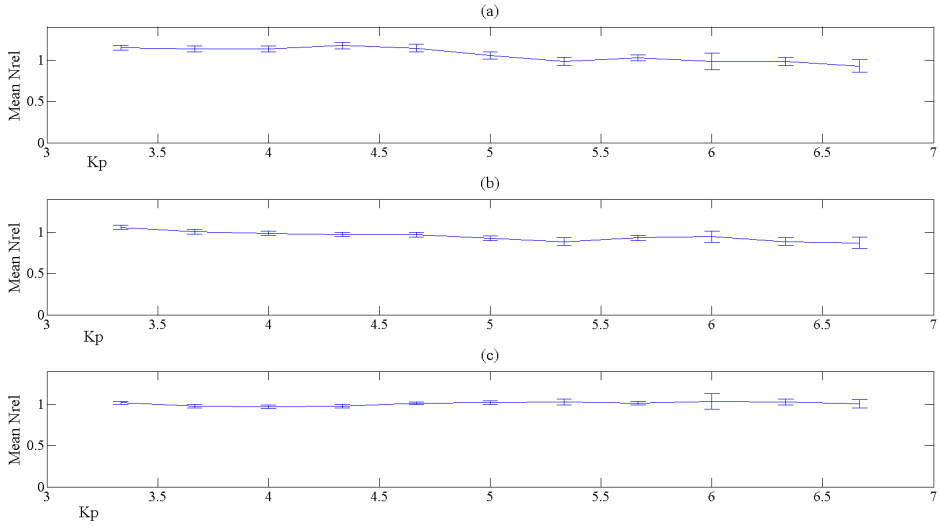

Figure 4.4: Kp and mean N_{rel} for Kp=3+ - 7-. (a) 93-99 km, (b) 87-93 km, (c) 81-87 km

Real time analysis

The differences between the real time and the middle time can be seen in figures 4.6(a)-4.6(c). From the 11th of November to the 11th of August 2013 this differences were found to have the averages magnitudes seen in table 4.2. On average the real times lies under 9 minutes away from the middle time in the 81-93 km region and 10.6 minutes away from the middle time at 93-96 km. This constitutes to 10-11.7% of the maximum of 1.5 hours. Although the mean number of meteors in table 4.1 are relatively high, they are all arriving within 180 minutes. Since the the meteor flux is randomly distributed by nature, this real time distribution around the middle time is also expected.
To see how these fluctuations in the real time affects wind measurements and analysis of these, there was performed an analysis of induced wind error and also a semidiurnal analysis.

Altitude (km)	**Average time error** (min)	**Average magniture of time error** (min)
81-86	0.19±10.77	8.9±7.5
86-93	0.33±10.47	8.5±7.4
93-99	0.358±13.8	10.6±8.8

Table 4.2: Average magnitude of time error at different altitudes 11. September 2012 - 11.August 2013. Error is the standard deviation.

Time induced wind error

The time induced wind errors are found in figures 4.6. On average the magnitude of these errors are displayed in table 4.4. This shows what is to be expected, which is that there is no general directionality of any significant size in the wind error, and that the time induced wind error averages out over the course of time.
The average magnitude of the wind error is shown in table 4.4 and it shows that the error is generally low. Due to how this error is found, it is natural that the wind-error is also connected to the time-error. The wind error we observe is also going to be related to the rate of change in the wind at the time. The larger the magnitude on the rate of change in wind speed is, the more significant a time error at that point will be. This can in fact be seen in the example plot below, figure 4.5. This is also one of the problems with this analysis. In order to do an accurate comparison with the rate of change, one should have more data points. By dividing the data into smaller bins, there will be fewer meteors in each segment, increasing the error in the wind itself and also the error in the measured wind. During this thesis the choice of three hours for each segment was made to have a higher general number of meteors, and also to make comparisons with Kp which is given for three hours at a time.
The standard deviations is also a measure of how much effect this error may have on a dataset. This can be compared to the standard deviation of the wind itself from the fit to the meteor data. The average of these can be seen in table 4.5, and it is higher for all regions then the standard deviation of the wind error.
An interesting number would then be how often the time induced wind error is larger then the error in the measured wind component itself. With the method and data to find the time induced wind error which is used in this gives a general number of 4.6% across all altitudes. What this is saying is that for 95.4% of the measured wind components this wind error will not be outside the error already invested in the data. Looking at each region individually, the percentage of significant error is 2.5% in the lowest region, 5.6% in the upper region and 5.7% in the highest region.

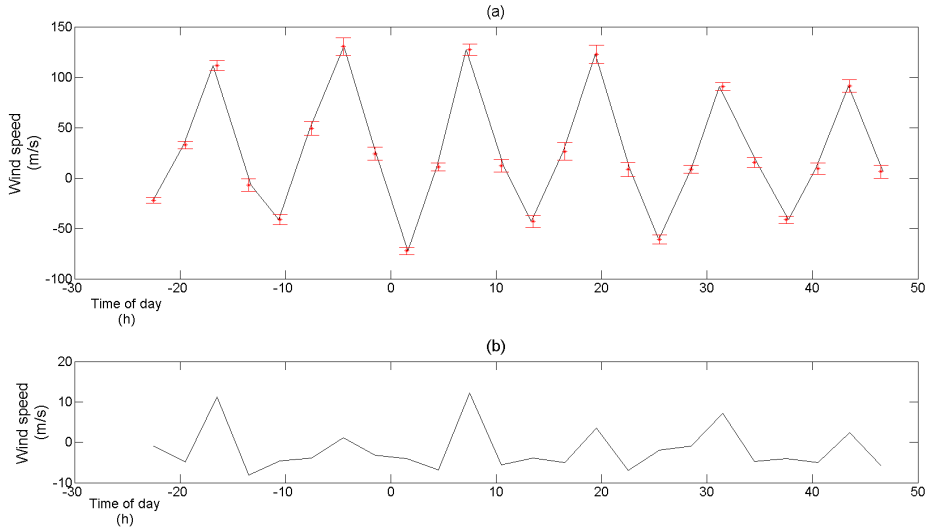

Figure 4.5: Example plot of the induced wind error from January 19th 2013, 93-99 km. (a) Blue: measured wind plotted and interpolated with real time. Red: Measured wind plotted at bin time with error from the measurement. (b) Difference between the measured wind and the linearly interpolated wind at bin time.

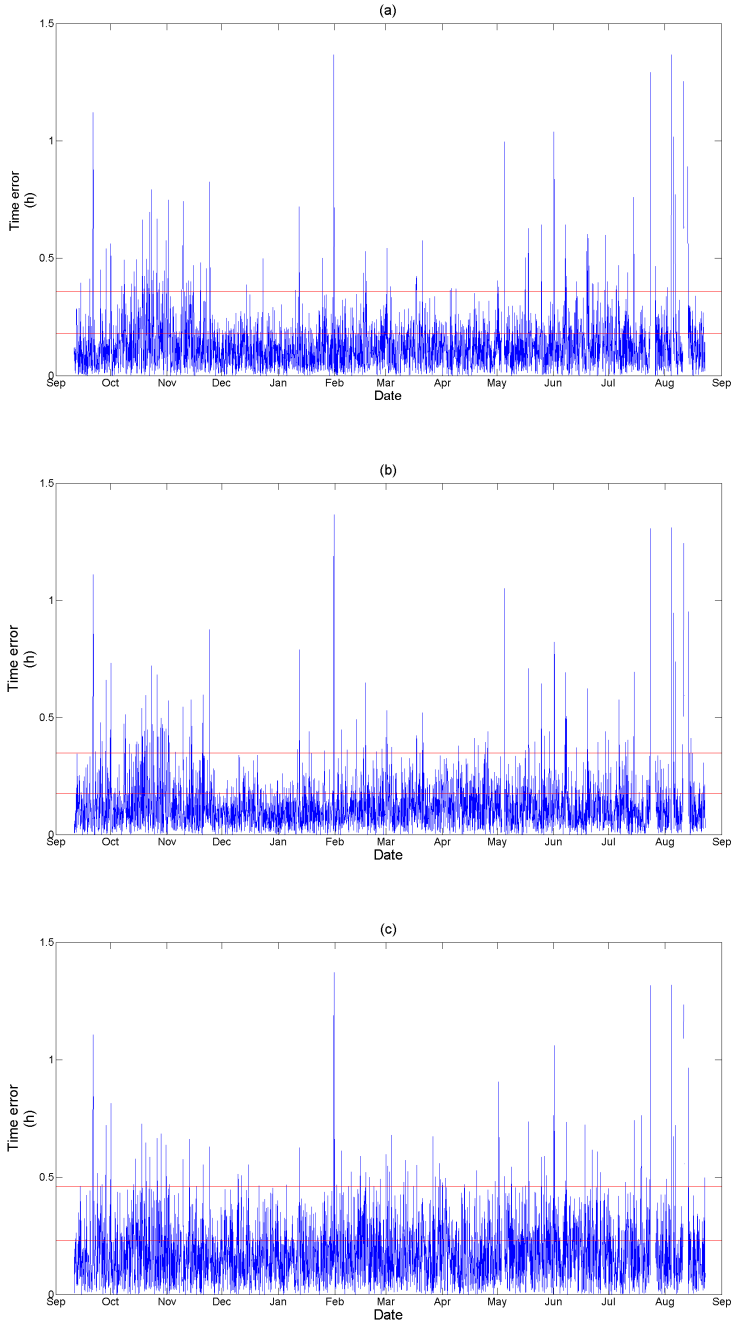

Figure 4.6: This plot shows the magnitude of the difference between real time and fixed time in the 93-96 km range. The red lines in the plot depict one and two standard deviations of this data. (a) 81-87 km, (b) 87-93 km, (c) 93-99 km.

Altitude (km)	**Average wind error zonal** (m/s)	**Average wind error meridional** (m/s)
81-86	-0.06±1.34	0.04±1.34
86-93	-0.01±1.62	0.01±1.57
93-99	-0.18±2.87	0.10±2.97

Table 4.3: List of averages of the wind error induced by differences between real time and middle time. The error in these numbers are the standard deviation in the data.

Altitude (km)	**Average zonal wind error magnitude** (m/s)	**Average meridional wind error magnitude** (m/s)
81-86	0.75±1.06	0.81±1.07
86-93	0.91±1.34	0.92±1.27
93-99	1.80±2.25	1.90±2.28

Table 4.4: Average magnitude of the wind error as result of real time deviation from middle time. Errors are standard deviations from the data.

Altitude	**Zonal**	**Meridional**
(km)	(m/s)	(m/s)
81-86	2.20	2.11
86-93	1.91	1.87
93-99	3.80	3.83

Table 4.5: This table contains the mean standard deviation from the fitting of the wind data points.

Correlation between number of meteors and time error

In order to see what impact the number of meteors have on the time error, it has been plotted in figure 4.7. The average magnitude of the time error is shown for different values of N at that time. There is a tendency for the time error to be higher the lower the number of meteors is. The standard mean error (SME) decreases with the number of meteors, as is to be expected.
In this case the standard deviation itself is a measure of the error in arrival time when using middle time, figure 4.8 also suggests a higher difference between the real time and the middle time when the number of meteors are low. The decrease in standard deviation gives the same information about the difference between real time and the middle time.

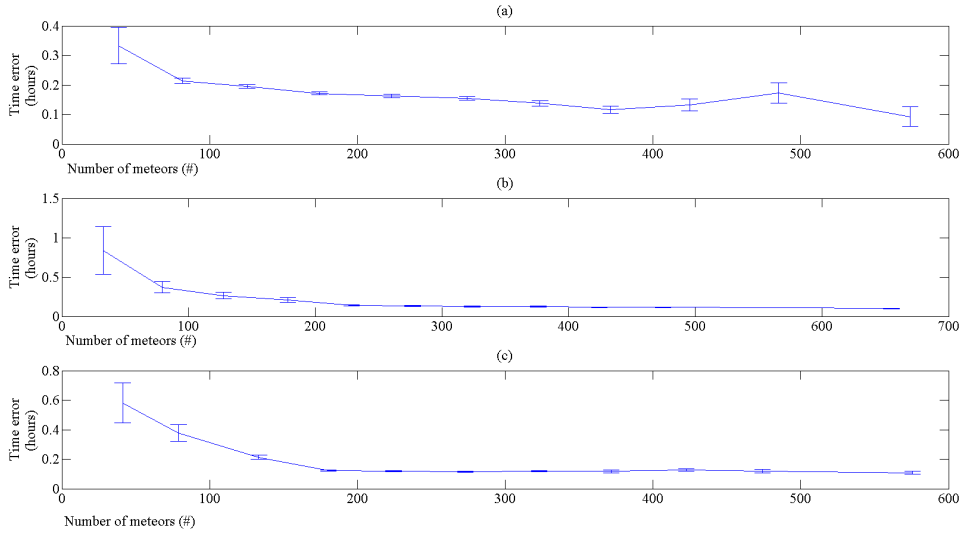

Figure 4.7: The time errors have been sorted after number of meteors, as 0-50, 50-100, ... 450-500 and >500. Both the average magnitude of the time error and the average of N have been found for each segment, so the time errors are plotted at their respective mean N. The errorbars show the standard mean error of the real time used for each average. Altitudes: (a) 93-99 km, (b) 87-93 km, (c) 81-87 km.

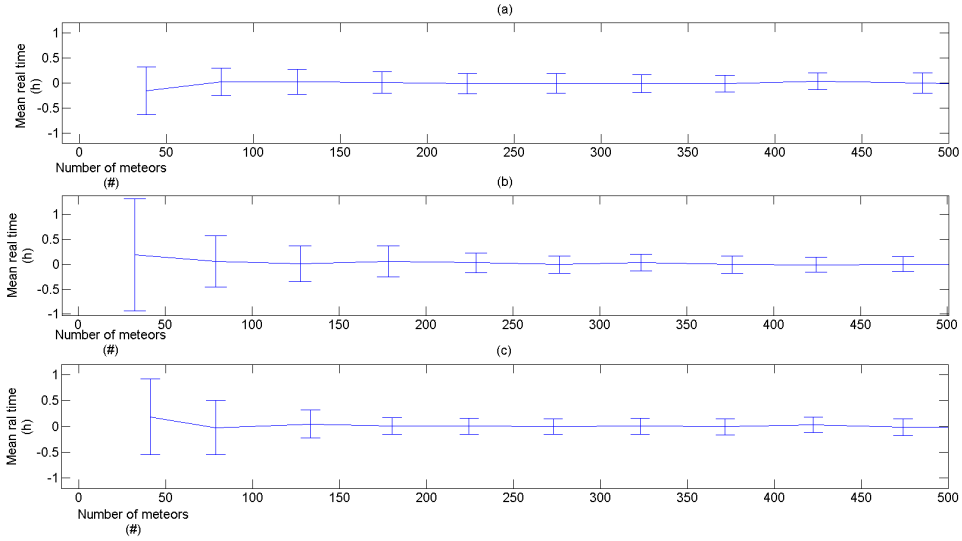

Figure 4.8: The time errors have been sorted after number of meteors, as 0-50, 50-100, ... 450-500 and >500. The real time and the number of meteors were averaged and plotted at their real number in the graphs. The errorbars show the standard deviation of the real times used in each average. Altitudes: (a) 93-99 km, (b) 87-93 km, (c) 81-87 km.

Semidiurnal analysis, 3 hour bins, Sept. 11th 2012 - Aug. 11th 2013:

From the figures 4.10 and 4.11 it is clear that for most of the points the difference between using real time and middle time in the analysis is small. Seeing as the time induced wind error is within the error 95.4% of the time, and that each of the semidiurnal amplitudes is found on the basis of 24 data points, this is expected.
The only time the difference was relevant was on January 19th 2013, which becomes even clearer by looking at the difference between the amplitudes.In figure 4.9 it can be seen that this difference is found to be 35.9 m/s. The amplitudes found here were 30.7 m/s for the middle time analysis and 66.7 m/s for the real time analysis. Looking at figure 4.15 it does look like there is a burst of amplitude in the semidiurnal at this time, and the larger amplitude found by the real time analysis seems to be the most accurate.
The phases of the fitted waves can be seen in figure 4.14. The phases found show the same thing as the amplitude, that there is little to no difference between the two types of fit when looking at the overall behavior.

This point is one of 1005 results for the zonal semidiurnal amplitude, so all in all the difference is insignificant most of the time. However, the one point with a significant difference shows that at times there is a reason to consider using real time instead of middle time for an analysis. It all comes down to what sort of analysis that is to be done and how accurate data one needs. For a general description of how the amplitude of the Semidiurnal is changing over the course of a year, both of the methods would work fine. For a detailed description of the semidiurnal on a daily basis, there is good reason to consider using real time instead. It is fairly easily implemented, and the extra time for an analysis like this to run with the real time instead of the middle time is not much, even with this amount of data.
A reason for why the effect is so small in this analysis may be that the meteor count rate with the SKiYMET radar used for the collection of data is high. It is a 35 kW radar, compared to the normal effect of 6 kW [Hoc01]. This means it is able to detect more meteors then what is to be expected from lower powered radars. When the meteor count is low we have already seen that the time error is generally larger in magnitude, so there is reason to believe that analyses using lower effect radars should consider using real time instead of bin time. Especially when comparing results with analyses done with higher power radars.

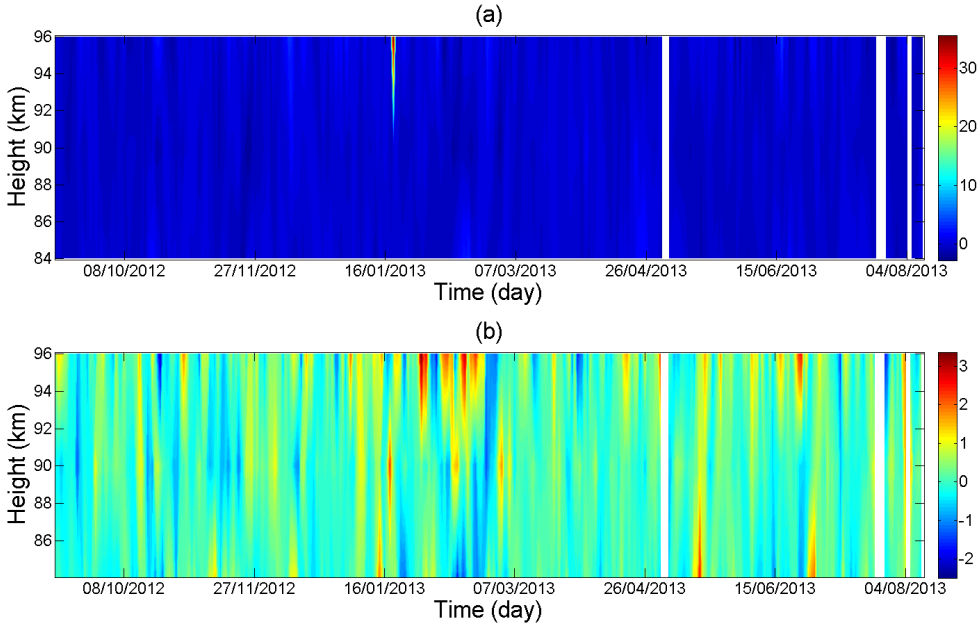

Figure 4.9: Difference between the amplitudes found in figure 4.10. The difference is the amplitude found using real time minus the amplitude found using middle time. (a) Zonal semidiurnal differences. (b) Meridional semidiurnal differences.

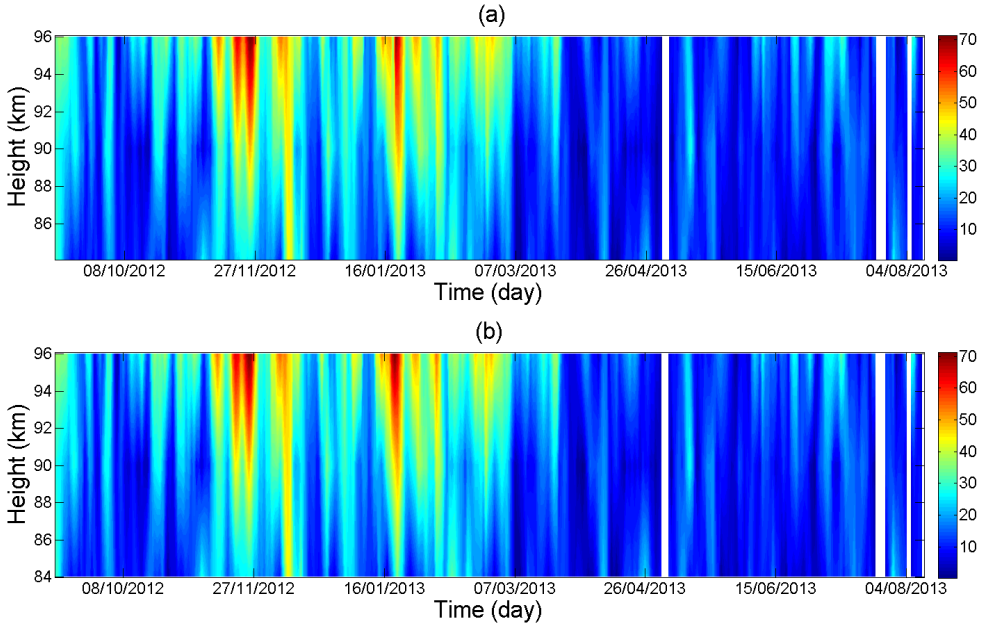

Figure 4.10: Amplitudes found for the zonal semidiurnal tide Sept. 11th 2012 - Aug 11th 2013. (a) Amplitudes found using middle times. (b) Amplitudes found using real times.

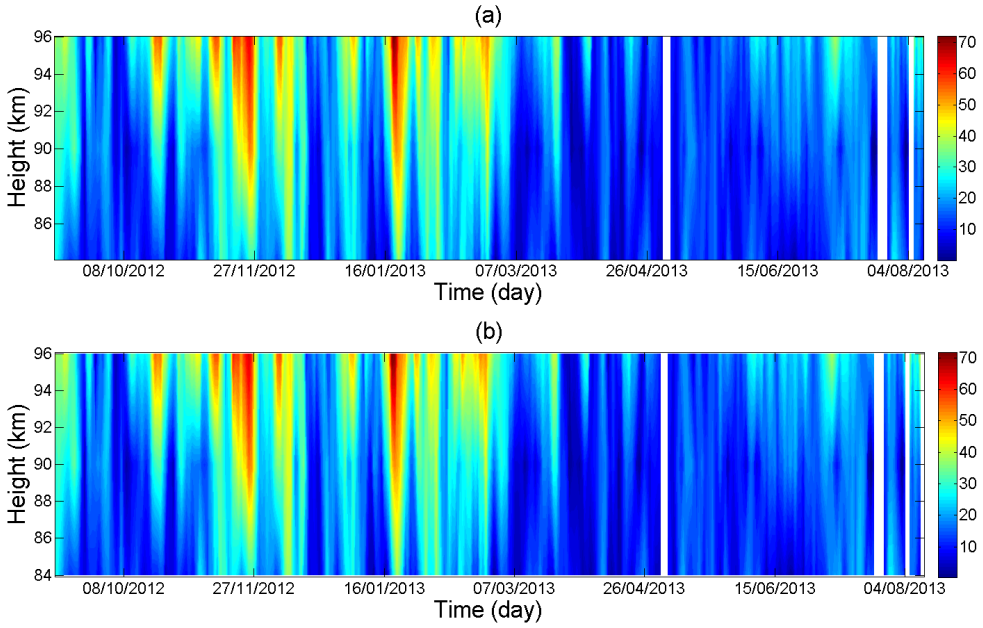

Figure 4.11: Amplitudes found for the meridional semidiurnal tide Sept. 11th 2012 - Aug 11th 2013. (a) Amplitudes found using middle times. (b) Amplitudes found using real times.

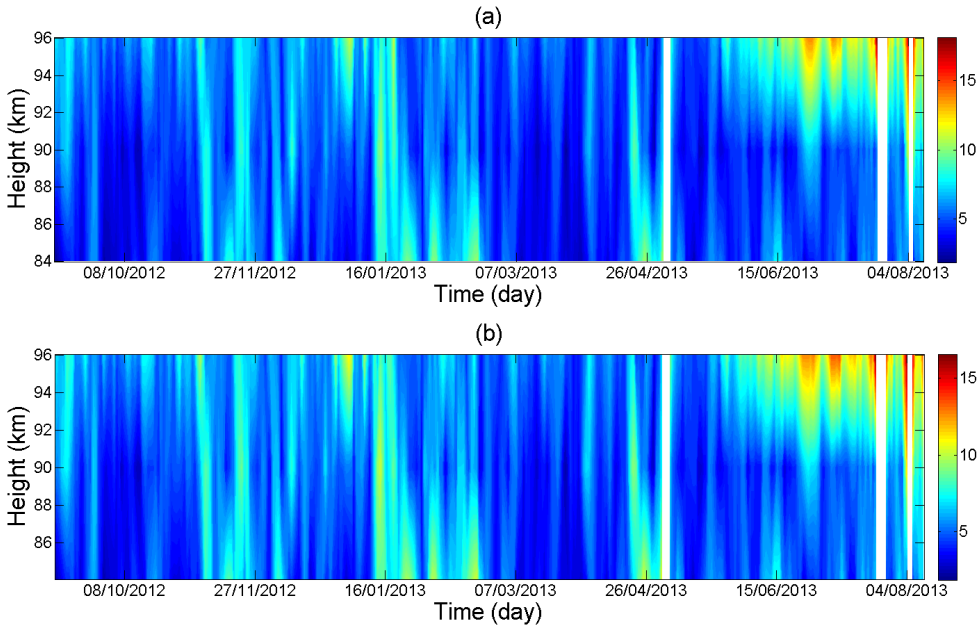

Figure 4.12: σ-error of the fitted amplitudes found in figure 4.10. (a) Middle time. (b) Real time.

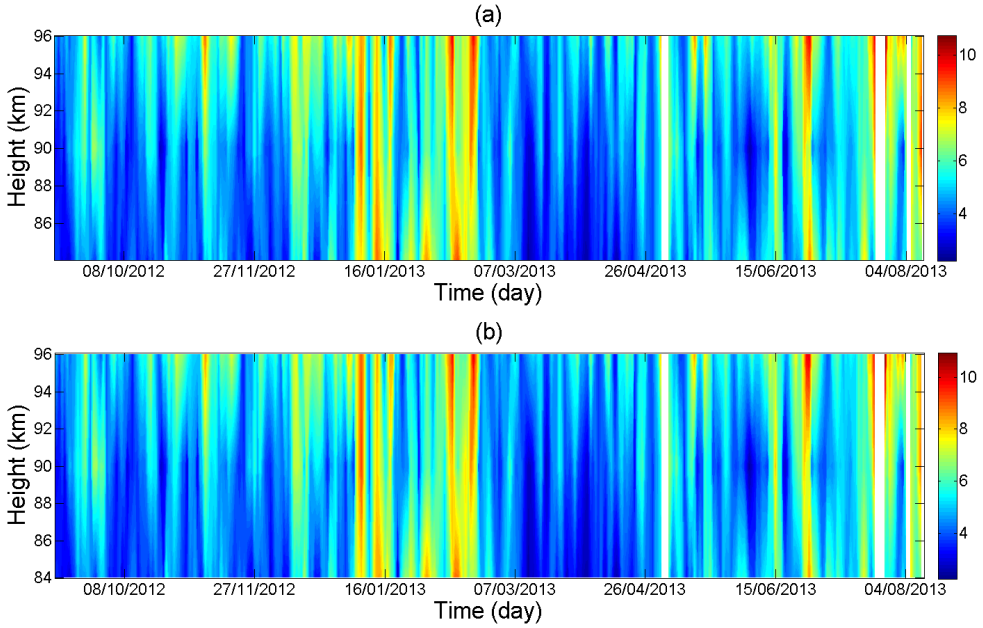

Figure 4.13: σ-error of the fitted amplitudes found in figure 4.11 (a) Middle time. (b) Real time

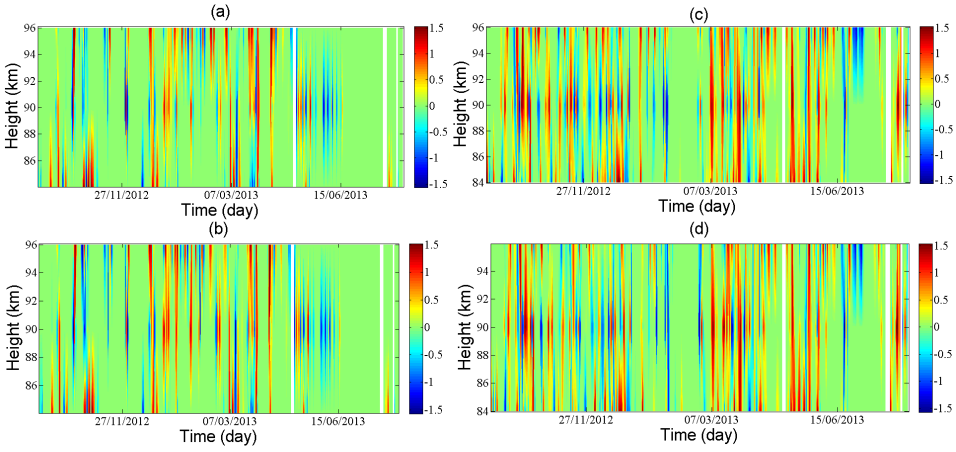

Figure 4.14: Phase of the semidiurnal waves fitted from 11.092012 - 11.08.2013. (a)Zonal, real time, (b) Zonal, bin time, (c) Meridional, real time, (d) Meridional, bin time

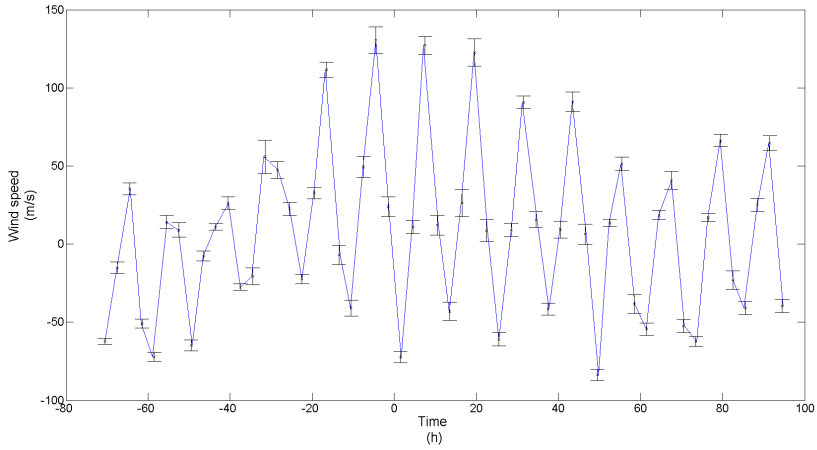

Figure 4.15: Plot of the zonal component of the wind at 93-99 km around 19.01.2013.

Semidiurnal analysis, 1 hour bins, October 2013: For this analysis, the wind components were calculated using 1 hour bins at altitudes 81-84, 84-87, 87-90, 90-93, 93-96, 96-99. This time the analyzed period was October. The results can be seen in figures 4.18 and 4.18, with errors in figures 4.19 and 4.20 . The differences between these amplitudes are plotted in figure 4.16. The phases can be seen in figure 4.21
As in the analysis with 3-hour bins there is one day with a large difference between the two approaches. This is the only time the difference between the two is significant, and it occurs on October 23rd, 96-99 km. This time the difference in the real time and bin time amplitudes is 19m/s. As with the first semidiurnal analysis this does mean that there may be a small difference between using the two approaches, however it may or may not affect the work done based on what the purpose of the analysis is.

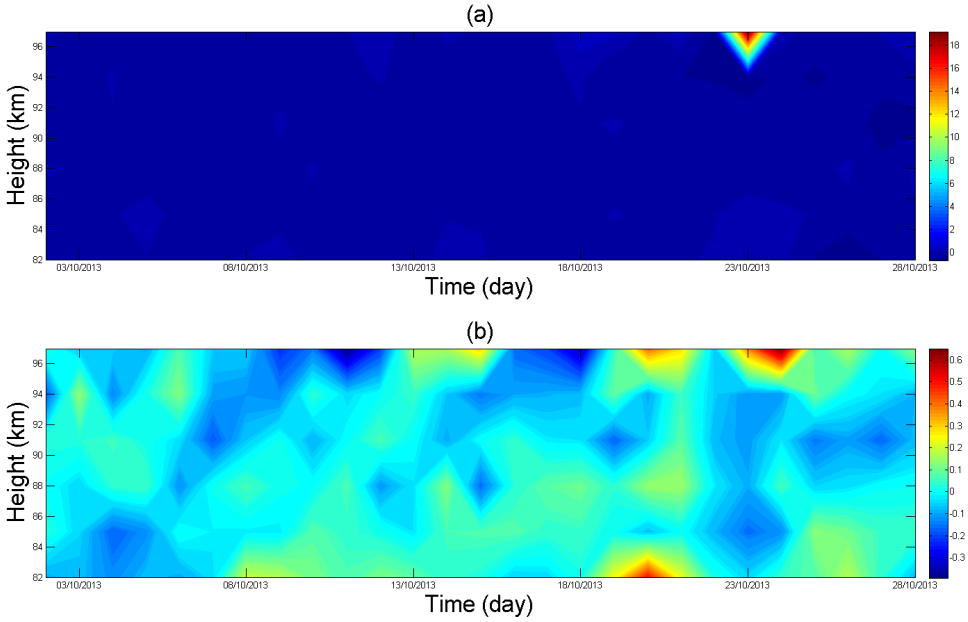

Figure 4.16: Difference between the semidiurnal amplitudes found for October 2013 using real time and middle time. (a) Zonal semidiurnal differences. (b) Meridional semidiurnal differences.

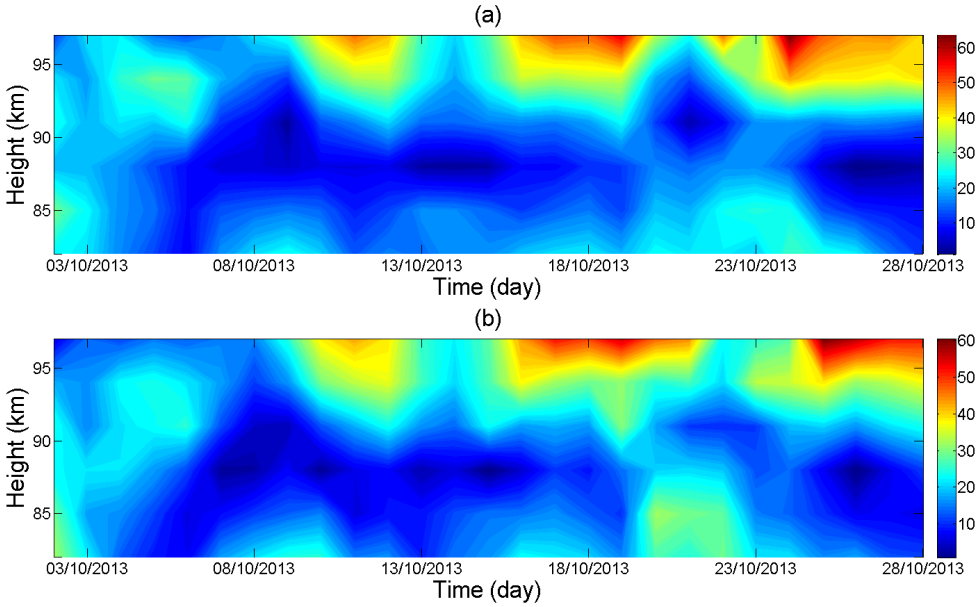

Figure 4.17: Amplitudes found for the semidiurnal tide October 2013 using fixed hourly time points. (a) Zonal, (b) Meridional

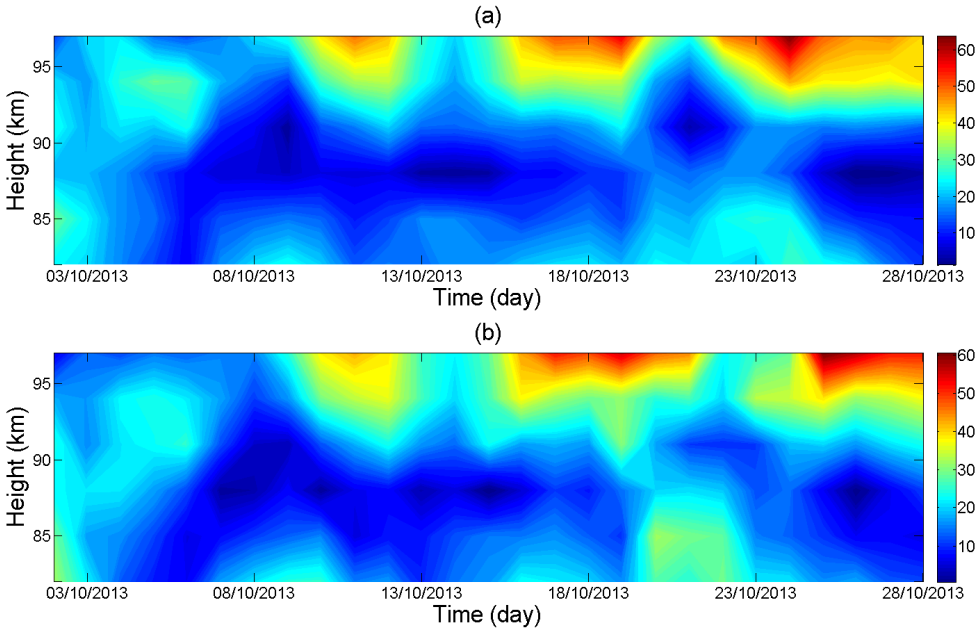

Figure 4.18: Amplitudes found for the semidiurnal side October 2013 using average time points. (a) Zonal, (b) Meridional

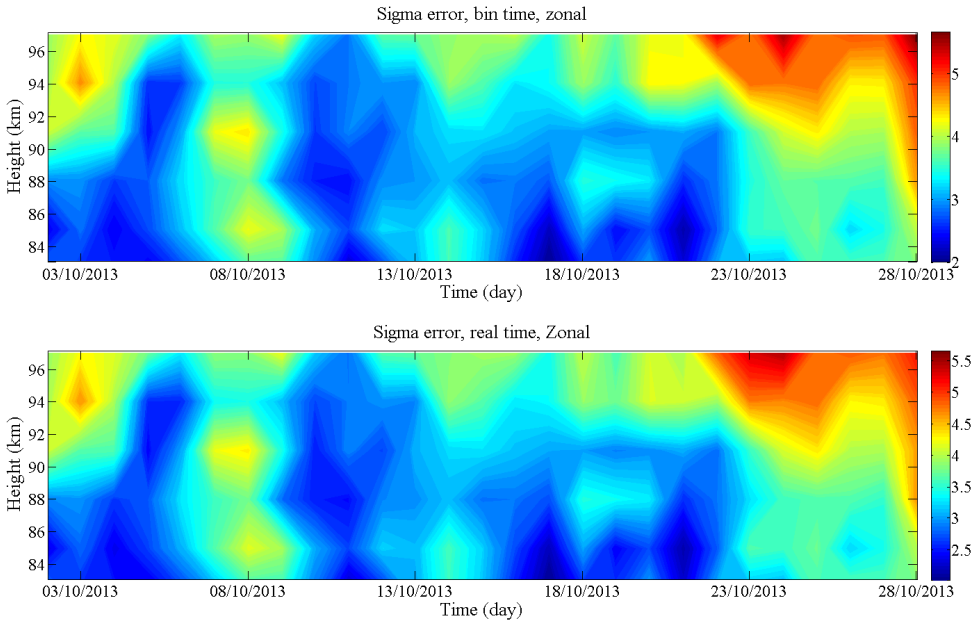

Figure 4.19: Zonal σ error of the amplitudes in figures 4.18 and 4.17. (a) Bin time, (b) Real time

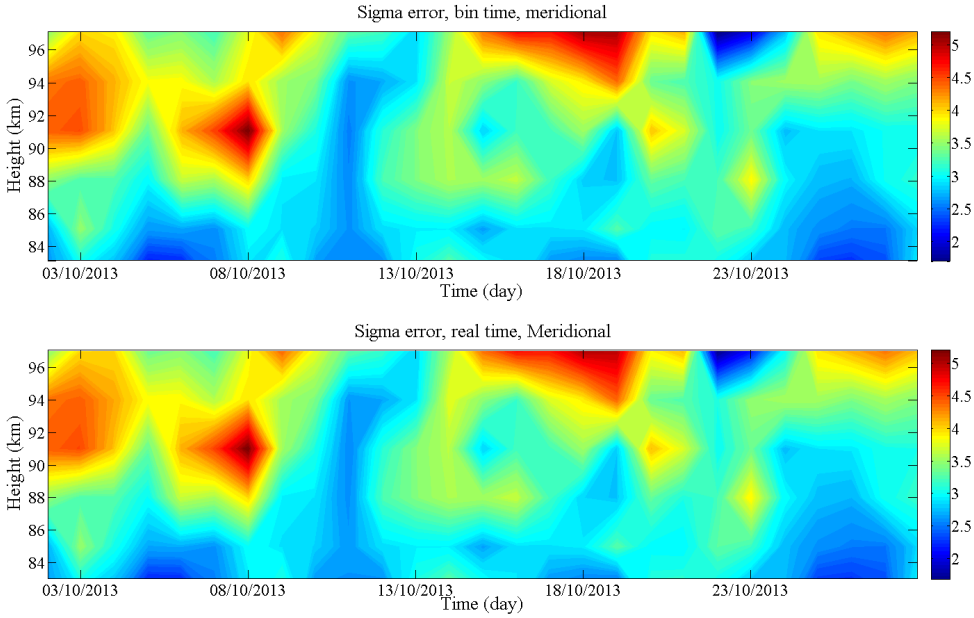

Figure 4.20: Meridional σ error of the amplitudes in figures 4.18 and 4.17. (a) Bin time, (b) Real time

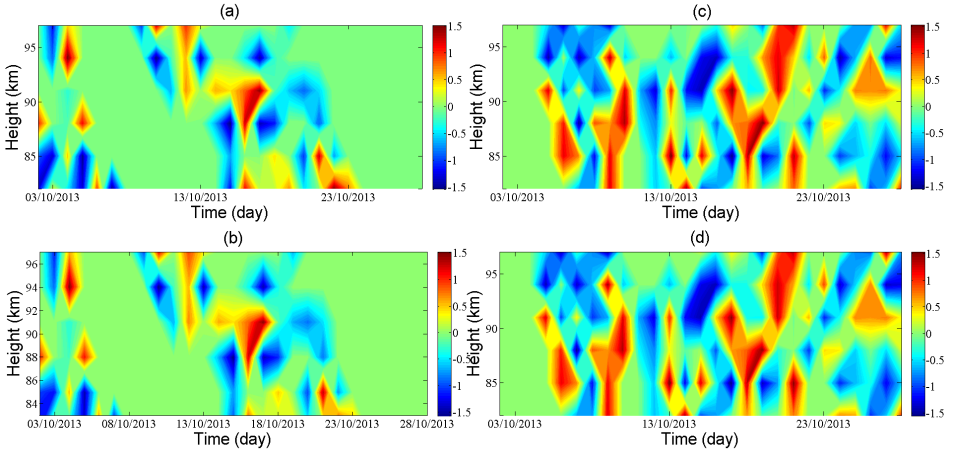

Figure 4.21: Phase of the semidiurnal tide October 2013 using 1-hour bins. (a) Zonal, real time, (b) Zonal, bin time, (c) Meridional, real time, (d) Meridional, bin time.

Chapter 5

Conclusion and further work

This thesis has shown that when Kp>4+, there is a slight tendency of a dropout in the number of meteors detected by the SKiYMET radar. This is likely caused by the increase in the background radiation caused by auroral precipitation. The meteor uses the background ionization as reference for meteor detection, and so with a background that is higher than usual it will have more trouble detecting the meteors.
When finding wind components using data from a SKiYMET radar, the real time for these components may vary significantly from the bin time when the number of meteors detected is low. On average the magnitude of the difference between real time and bin time was found to be 9-10.6 minutes in the 81-99 km region, using 3 hour bins. By using bin time, this time error will induce an error in the wind components. By linearly interpolating the real time components and comparing the measured component to the linear interpolant at bin time, the average magnitude of the error was found to be greater then measuring error in 4.6% of the measured components. In the 81-87 km region this was as low as 2.7%, however in the 87-99 km region a significant induced time error was found in 5.65% of the wind measurements.
By doing a semidiurnal analysis using both real time and bin time the difference between these two approaches was investigated. The two approaches yielded a significant difference between results for the semidiurnal amplitude once during a 11 month analysis using 3 hour bins and 6 km altitude bins. An analysis of October using 1 hour bins and 3 km altitude bins also produced one significant difference between the two. Whether or not to use real time or bin time for analysis of data from a 35 kW SKiYMET meteor radar is therefore something that needs to decided by the user itself. For general behavior of the atmospheric winds, where several days of data is used for analysis, the bin time will likely be sufficiently accurate.
A 35 kW system as the one that is located in Trondheim, will be detecting more meteors then less powerful systems (in general the power is 6 kW [Hoc01]), so the occurrence of low meteor counts will be rarer and less influential when doing analysis on several days of data. Comparing this system to the systems like a VHF radar, the SKiYMET at Dragvoll collects typically 8000 meteors in the winter and 16000 meteors in the summer, while the

VHF system peaks at around 7000 meteors in the summer [YASM09b]. I would therefore recommend the users of less powerful systems to consider the effect on their own analyses from time induced error.
When comparing winds from different systems or locations, a consistent time base should be used so that any change can be ascribed to the system or location differences.

Bibliography

[For09] J.M Forbes. Vertical coupling of the semidiurnal tide in the earth's atmosphere. *Annual reviews*, 2009.

[Hoc01] et. al Hocking, W.K. Real time determination of meteor-related parameters utilizing modern technology. *Journal of Atmospheric and Solar-Terrestrial Physics*, 63, 2001.

[Jur85] Adolph S Jursa. *Handbook of geophysics and the space environment*. Air Force Geophysics Laboratory Springfield, VA, 1985.

[Lie09] R.S. Lieberman. An overview of middle atmosphere tides. In *HEPPA (International high energy particle precipitation in the atmosphere workshop*, Colorado, USA, 2009.

[Lin79] R.S. Lindzen. Atmospheric tides. *Annual reviews*, 1979.

[SBHM10] David J Sandford, Charlotte L Beldon, Robert E Hibbins, and Nicholas J Mitchell. Dynamics of the antarctic and arctic mesosphere and lower thermosphere–part 1: Mean winds. *Atmospheric Chemistry and Physics*, 10(21):10273–10289, 2010.

[SWP] Space Weather Prediction Centre SWPC. http://www.swpc.noaa.gov/.

[TVS+09] Esa Turunen, Pekka T Verronen, Annika Seppälä, Craig J Rodger, Mark A Clilverd, Johanna Tamminen, Carl-Fredrik Enell, and Thomas Ulich. Impact of different energies of precipitating particles on no$_x$ generation in the middle and upper atmosphere during geomagnetic storms. *Journal of Atmospheric and Solar-Terrestrial Physics*, 71(10):1176–1189, 2009.

[YASM09a] PT Younger, Ivan Astin, David J Sandford, and Nicholas J Mitchell. The sporadic radiant and distribution of meteors in the atmosphere as observed by vhf radar at arctic, antarctic and equatorial latitudes. 27(7):2831–2841, 2009.

[YASM09b] PT Younger, Ivan Astin, David J Sandford, and Nicholas J Mitchell. The sporadic radiant and distribution of meteors in the atmosphere as observed by vhf radar at arctic, antarctic and equatorial latitudes. In *Annales Geophysicae*, volume 27, pages 2831–2841, 2009.